Portugaliae Electrochimica Acta 2017, 35(1), 39-51

DOI: 10.4152/pea.201701039

PORTUGALIAE ELECTROCHIMICA ACTA
ISSN 1647-1571

Experimental and Theoretical Study of Some N-pyridinium Salt Derivatives as Corrosion Inhibitors for Mild-steel in 1 M H_2SO_4

Mehdi S. Shihab* and Atheer F. Mahmood

Department of Chemistry, College of Science, Alnahrain University, Baghdad, Iraq

Received September 11, 2015; accepted November 11, 2016

Abstract

N-pyridinium salt derivatives (1), (2), (3), (4) and (5) were prepared and their inhibition effect as corrosion inhibitors for mild steel was investigated in 1 M H_2SO_4 solution at 30 ^oC for 24 hs. The corrosion inhibiting action was studied using weight loss measurements. The results have revealed that the corrosion rate decreases, inhibition efficiencies increase and surface coverage degree increases with a higher inhibitor's concentration. Inhibition efficiencies for prepared N-pyridinium salt derivatives have the highest inhibiting efficiency even for a low concentration. The values of ΔG^o_{ads} are showing physisorption effect for all prepared compounds. Molecular modeling systems were achieved for the suggested inhibitors (1), (2), (3), (4) and (5). Theoretical calculations could be used as a useful tool to obtain information for explaining the mechanism and nature of interaction between the metal surface and the organic molecule as a corrosion inhibitor.

***Keywords**:* corrosion inhibitor, inhibition efficiencies, physisorption, molecular modeling.

Introduction

Corrosion of materials has kept getting significance in the wide fields of technology. Corrosion inhibition researches are assiduous to find variant and efficient ways of protecting the metals against corrosion. The mechanistic basis of corrosion inhibitors depends on the specific interaction between certain atoms in the inhibitors with the corroded sites on the metal surface. These atoms, such as nitrogen, oxygen and sulphur have a main role in this interaction via donating their free electron pairs [1, 2]. Schiff bases found interest applications as corrosion inhibitors in carbon steels [3, 4], and other metals [5, 6]. Literature has revealed that alkyl quaternary ammonium compounds are important as inhibitor additives in acidic media to reduce the corrosion process of iron and steel [7, 8].

* Corresponding author. E-mail address: mehdi_shihab@yahoo.com

Theoretical chemistry, such as quantum chemical calculations has been used to illustrate the mechanism of corrosion inhibition [9, 10]. Theoretical calculation could be a useful tool on finding the relationship between the corrosion inhibition efficiency and a number of quantum parameters, which will determine the demand of a molecular model system of effective corrosion inhibitors.
In the present work, the inhibition of corrosion of mild steel in 1 M H_2SO_4, in the presence of prepared N-pyridinium salt derivatives, has been evaluated at 30 ^oC, and at different concentrations of inhibitor, using weight loss method. The results of measurements showed excellent inhibitive efficiency of the corrosion inhibitors. The relationship between high efficiencies and molecular structure of the corrosion inhibitors is studied using quantum chemical calculations at PM3 level.

Experimental testing

Materials

The mild steel sheet used had the composition percentages of 0.002% P, 0.288% Mn, 0.03% C, 0.0154% S, 0.0199% Cr, 0.002% Mo, 0.065% Cu, 0.0005% V, and the remainder iron. The mild steel sheet was mechanically press-cut into disc shape with a diameter of 2.5 cm and thickness sheet 0.05 cm. These disc shapes were polished with emery papers ranging from 500 to 1500 grades, to get a highly smooth surface. However, surface treatments of the mild steel involved degreasing in absolute ethanol and drying in acetone.
The treated specimens were then kept in a moisture-free desiccator before their use in corrosion studies.
N-pyridinium salt derivative inhibitors, namely: 1-benzyl-4-(2-(4-(dimethylamino) benzylidene) hydrazinecarbonyl) pyridinium chloride (1), 1-benzyl-4-(2-(4-nitrobenzylidene) hydrazinecarbonyl) pyridinium chloride (2), 1-benzyl-4-(2-(1,5-diphenylpenta-1,4-dien-3-ylidene) hydrazinecarbonyl) pyridinium chloride (3), 1-benzyl-4-(2-(1,3-diphenylallylidene) hydrazinecarbonyl) pyridinium chloride (4), and 1-benzyl-4-(2-(propan-2-ylidene) hydrazinecarbonyl) pyridinium chloride (5), were synthesized as follows: first, the preparation of Schiff's base was carried out by condensation reaction between the isonicotinic hydrazide and a ketone or an aldehyde [11]; then, a mixture of Schiff's base compound (0.01 mol), abs. ethanol (20 mL) and benzyl chloride (0.01 mol) was refluxed for 50 h; after cooling to room temperature, the precipitate was filtered and dried; the product of N-pyridinium salt was two times washed with ethanol [12]. All prepared compounds were identified from melting point, FTIR (KBr disc) and ^{1}HNMR (DMSO-d_6) techniques. The molecular formula of the suggested inhibitors is shown in Scheme 1. N-pyridinium salt inhibitor's concentrations of 1×10^{-2} to 5×10^{-4} M were prepared in a solution of 1 M H_2SO_4 at 30 ^oC. A mixture of analytical grade 98% H_2SO_4 with distilled water was carried out to prepare 1 M H_2SO_4 aqueous solution.

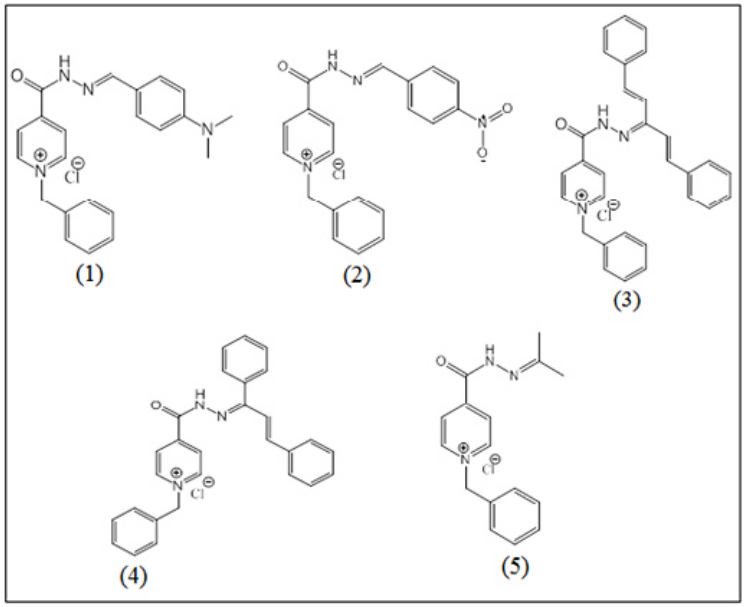

Scheme 1. Molecular structure of prepared N-pyridinium salt inhibitors.

Weight loss method

Initial weight of mild steel specimen was determined using an electronic balance as a starting step of the weight loss method. The specimens were pended and completely immersed in a proper beaker containing 1 M sulfuric acid, in the presence and absence of N-pyridinium salt inhibitor. The specimens were removed after 24 h exposure period at 30 ^{o}C, washed with water to remove any corrosion products, and finally washed with acetone. After that, they were dried and their weight was determined. Mass loss measurements were achieved using ASTM standard test method previously described [13, 14]. The measurements were carried out in duplicate to perform the reliability of the results, and the mean value of the weight loss was fixed in 2–3% data errors. Weight loss allowed calculation of the mean corrosion rate in mg cm^{-2} h^{-1}. The corrosion rate of mild steel was determined using the relationship (1) [15]:

$$W = \frac{\Delta m}{St} \qquad (1)$$

where Δm is the mass loss, S the area and t is the immersion period.

The inhibition efficiency percentage (E (%)) was calculated using the relationship (2) [16]:

$$E\% = \frac{W_{Corr} - W_{corr\,(inh)}}{W_{corr}}\ x\ 100 \qquad (2)$$

where W_{corr} and $W_{corr(inh)}$ are the corrosion rates of mild steel in the absence and presence of the inhibitor, respectively.

Basic information can be provided from the adsorption isotherms, to explain the interaction between the organic compounds and metal surfaces. Therefore, the degree of surface coverage values (θ) at different inhibitor concentrations in 1 M H_2SO_4 was achieved from weight loss measurements (θ = E (%)/100) at 30 ^{o}C, and tested with Langmuir isotherm relationship (3) [17]:

$$C/\theta = 1/K_{ads} + C \qquad (3)$$

where C is the concentration in M, and K_{ads} is the equilibrium constant of the adsorption process (4) [18]:

$$\text{Organic}_{(sol)} + xH_2O_{(ads)} \leftrightarrow \text{Organic}_{(ads)} + xH_2O_{(sol)} \qquad (4)$$

According to the Langmuir isotherm, K_{ads} values can be calculated from the intercepts of the straight line of plotting (C/θ versus C). K_{ads} is related to the standard free energy of adsorption, ΔG^{o}_{ads}, with the following eq. (5) (the value 55.5 is the molar concentration of water in the solution in M) [18]:

$$K_{ads} = \frac{1}{55.5} exp(-\frac{\Delta G_{ads}}{RT}) \qquad (5)$$

Theoretical calculations

Minimum energy calculations were performed using molecular mechanics/ MM+ level; then, the semi-empirical calculations were made with PM3 method [19]. For this purpose, the Hyperchem program [20] with complete geometry optimization was used. The geometry optimization of all suggested inhibitors was performed, and all geometric variables were optimized without any symmetry constraints, to get minimum energy structures. Most of the quantum chemical calculations of the inhibitors in gas phase showed good correlation with inhibition efficiency, and revealed to be a good tool to explain the differences in the efficiencies of the inhibitors [21, 22].

Table 1. Calculated quantum chemical parameters of suggested inhibitors, using PM3 method.

Inhibitor	HOMO (eV)	LUMO (eV)	ΔE (E_{LUMO}- E_{HOMO}) (eV)	μ(Debye)
(1)	-10.4705	-5.4120	5.0585	8.3
(2)	-12.3585	-5.7162	6.6423	13.9
(3)	-10.8947	-5.3949	5.4998	13.2
(4)	-11.0399	-5.4187	5.6212	12.6
(5)	-12.2342	-5.7243	6.5100	3.0

The comparison of the inhibition efficiencies of prepared compounds (1), (2), (3), (4) and (5) with that of the highest occupied molecular orbital (HOMO) and of the lowest unoccupied molecular orbital (LUMO), and other indices, will provide useful information to build a molecular model system of newly effective corrosion inhibitors. The optimized molecular structures calculated energies E_{HOMO}, E_{LUMO}, energy gap (ΔE, the lower value of it has, the higher stability is for the formed complex on the metal surface [23]) and other parameters are given in Table 1.

Results and discussion

The effect of the addition of N-pyridinium salt at various concentrations on mild steel corrosion in 1 M H_2SO_4 aqueous solutions is tested by weight loss measurements at 30 °C, after 24 h immersion. The corrosion parameters, such as inhibition efficiency (IE %) and corrosion rate at different concentrations of suggested inhibitors are presented in Table 2 and depicted in Fig. 1 (a, b), respectively.

Table 2. Corrosion parameters of mild steel in 1 M H_2SO_4 in the presence of different concentrations of N-pyridinium salt derivatives by weight loss measurements at 30 °C.

Concentration (M)	Corrosion rate ($mg.cm^{-2}.h^{-1}$)	IE%	Θ	$\Delta G°_{ads}$ ($kJ.\ mol^{-1}$)
Blank	0.631	-	-	-
(1)				
5×10^{-4}	0.118	81.30	0.813	-32.02 (R^2=0.999)
1×10^{-3}	0.109	82.73	0.827	
5×10^{-3}	0.028	95.56	0.956	
1×10^{-2}	0.008	98.73	0.987	
(2)				
5×10^{-4}	0.476	24.44	0.246	-26.83 (R^2=0.996)
1×10^{-3}	0.363	42.45	0.425	
5×10^{-3}	0.076	87.95	0.879	
1×10^{-2}	0.056	91.11	0.911	
(3)				
5×10^{-4}	0.060	90.50	0.905	-36.04 (R^2=0.999)
1×10^{-3}	0.007	98.89	0.989	
5×10^{-3}	0.010	98.41	0.986	
1×10^{-2}	0.003	99.52	0.995	
(4)				
5×10^{-4}	0.008	98.78	0.987	-38.70 (R^2=0.999)
1×10^{-3}	0.009	98.72	0.987	
5×10^{-3}	0.008	98.78	0.988	
1×10^{-2}	0.003	99.52	0.995	
(5)				
5×10^{-4}	0.062	90.17	0.902	-34.14 (R^2=0.999)
1×10^{-3}	0.042	93.40	0.934	
5×10^{-3}	0.016	97.51	0.975	
1×10^{-2}	0.003	99.52	0.995	

These results revealed that the mild steel corrosion was decelerated in the presence of suggested inhibitors in 1 M H_2SO_4 at all concentrations that were used in the present study. However the rate of corrosion of mild steel specimen in 1 M H_2SO_4 was high after 24 h without inhibitor.

It's clear that these data denote that inhibition efficiency increases and corrosion rate decreases with higher concentrations of all the inhibitors. This remarkable behavior can be explained by the increased adsorption and new coverage protection of inhibitors on the mild steel surface when we increase the inhibitor's concentration. The inhibitive action, as well as the adsorption process, can be attributed to the sort of functional group present in the molecular structure of the suggested inhibitors (1-5).

By using the Langmuir adsorption isotherm relationship (2), the experimental values of standard free energy of adsorption in Table 2 are negative. Negative

values indicate that the processes of adsorption of all suggested inhibitors (1-5) on the mild steel surface were spontaneous, after 24 h immersion at 30 °C. The magnitude of $\Delta G°_{ads}$ can explain effective interaction between the suggested inhibitors and the metal surface.
Also, the values of $\Delta G°_{ads}$ are lower than -40 kJ/ mol; that is referred to the adsorption type regarded as physisorption, in which the electronic structure of the molecule is disturbed when the adsorption causes electrostatic interaction between organic charged molecules and the charged metal, which protects the metal from corrosive attack [24-27]. In the process of adsorption, the first step of corrosion inhibition is the transport of the inhibitor to the metal surface; the second is the adsorption on the metal surface. The adsorbed inhibitor on the metal surface may result in the formation of an insoluble metal complex adhesion on the surface of the *metal*.

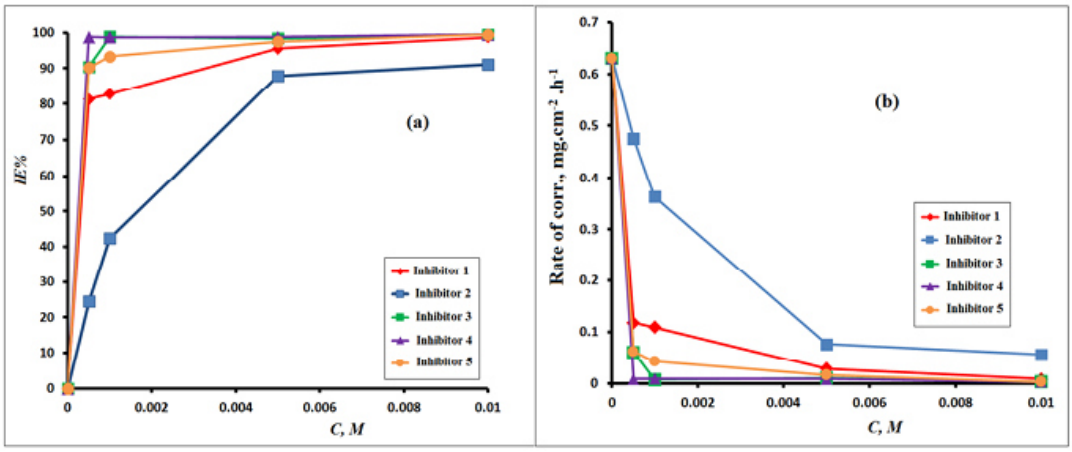

Figure 1. Effect of inhibitor concentration on the inhibition efficiency (a), and rate of corrosion (b) for mild steel, obtained at 30 °C in 1 M H_2SO_4, containing different concentrations of the suggested inhibitors.

In an acid solution, the iron metal reacts with the acidic environment to produce dissolving $Fe2^+$ ion and hydrogen gas. The resulting Fe^{2+} ion coordinates with water molecules to form $Fe^{2+}(H_2O)_x$. The anodic reaction may be represented by eq. (6) [27]:

$$Fe + xH_2O + 2H^+ \rightarrow Fe^{2+}(H_2O)_x + H_2 \qquad (6)$$

Then, approaching the inhibitor's molecules with their own high electron density sites to the metal surface could influence its adsorption behavior. Thus, the probability to form a metal-inhibitor complex could be achieved, as showed in eq. (7) [28]:

$$Fe^{2+}(H_2O)_x + Inh_{sol} \rightarrow xH_2O + [(Fe\text{-}Inh)^{+2}]_{ads} \text{ (a complex)} \qquad (7)$$

The formation of the complex creates a protective barrier between the metal surface and the environment. Thus, the process of anodic dissolution is driven by the adsorbed inhibitor molecules.

Semi-empirical calculations with PM3 level were used to study the relationship between a molecular structure model and experimental results of inhibition efficiency of the prepared inhibitors.
All the theoretical quantum calculations were performed for suggested inhibitors (1), (2), (3), (4) and (5), using more energetically stable conformations (see Fig. 2) which are shown to be non-planar for the total area of the molecular model of the suggested inhibitors.

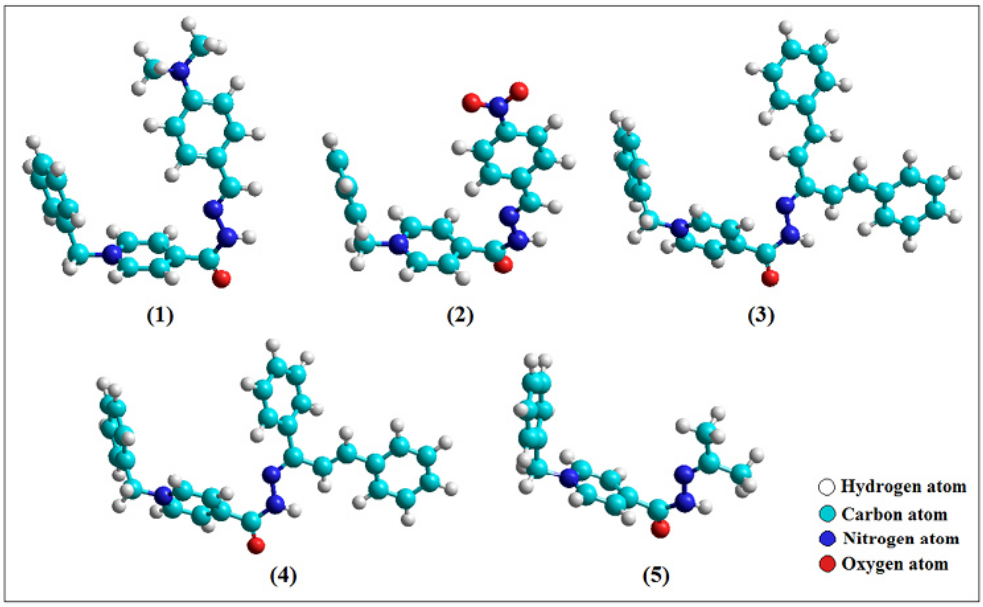

Figure 2. Energetically stable conformations of the suggested inhibitors (1), (2), (3), (4) and (5) with PM3 method.

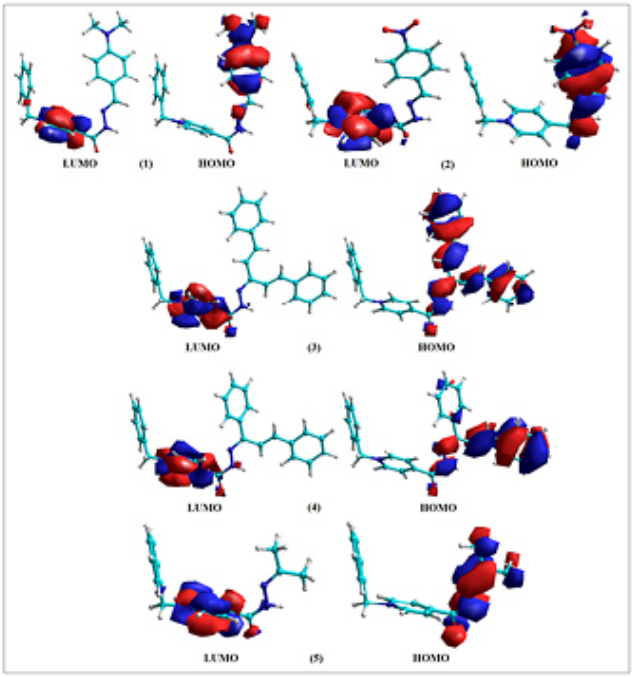

Figure 3. The frontier molecular orbital density distributions (HOMO and LUMO) for the suggested inhibitors (1), (2), (3), (4) and (5) by using PM3 method.

The calculated quantum chemical parameters of suggested inhibitors are listed in Table 1.
Isosurface maps of HOMO and LUMO for suggested inhibitors (1), (2), (3), (4) and (5) are depicted in Fig. 3.
The presence of N atoms in the suggested inhibitors makes the electronic density of the HOMO and LUMO completely localized on N of (C=N) and N of pyridinium ring for all molecules. This means that the electronic density of the N atom in the imine group acts as donor for the intermolecular interaction with the environments. The various values of dipole moments for the suggested inhibitors (1), (2), (3), (4) and (5) (see Table 1) could arise from the different electronegativity of atoms that were distributed in each molecule. These results can improve the dipole-dipole interactions between the organic molecules and the mild steel surface.
Electrostatic potential maps for suggested inhibitors (1), (2), (3), (4) and (5) are shown in Fig. 4, which reflect the different magnitude of calculated dipole moments.

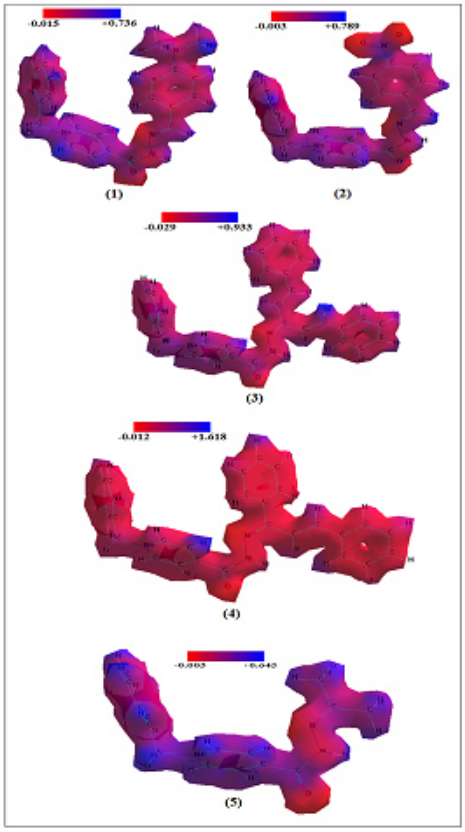

Figure 4. Electrostatic potential maps for the suggested inhibitors (1), (2), (3), (4) and (5) by using PM3 method.

This figure reveals the location of the high electron density on specific atoms (N and O atoms). These atoms can be said to be under the effect of dipole-dipole interactions between organic molecule and metal surface.
On the basis of the above, the obtained experimental data and theoretical calculations could coincide due to different molecular structures, which drive the inhibiting effect of the suggested inhibitors.

There are electronic and spatial distribution effects that explain the role of the molecular structure on the inhibition efficiency of the suggested inhibitors. The concentration of the electron density on the atoms N (C=N) and O (C=O) of the suggested inhibitors gave them an excellent inhibition effect (see Table 2). The optimized geometry of all molecules (see Fig. 2) enabled the special distribution of atoms in space, so that atoms with high electron density get closer to the metal surface and that, in its turn, improves the physisorption at high concentrations. With this spatial distribution, the positive pyridinium species may protect Fe surface, thus forming positive sites, as a result of the anodic process. This, in turn, may affect the adsorption of the inhibitor's molecules.
Based-on experimental and theoretical results, we demonstrate the orders below:

- (5), (4), (3) > (1) > (2) (Related to IE (%) (at 0.001 M), see Table 2)
- (4) > (3) > (5) > (1) > (2) (Related to ΔG^{o}_{ads}, see Table 2)
- (1) > (3) > (4) > (5) > (2) (Related to ΔE (energy gap), see Table 1).

Generally, we have got a relative consistency between the experimental and theoretical results for (1), (3), (4) and (5), showing high inhibition efficiencies due to the electronic effects of the atoms N (C=N) and O (C=O), and supported by the contribution of donating groups through resonance ($-N(CH_3)_2$ and -CH=CH-) and inductive effects ($-CH_3$).Regarding the compound (2), the results were completely consistent with decreasing values of IE%, ΔG^{o}_{ads} and ΔE, due to the presence of the withdrawing group ($-NO_2$). We can conclude that the theoretical calculations provided molecular modeling systems to understand the correlation between molecular structure and inhibition corrosion.
Finally, molecular mechanics (MM+) method and quantum calculations with PM3 method were also used to suggest mechanism of interaction between the organic molecule and the metal surface. The donor-acceptor adsorption interaction is the most reactive reaction between an organic inhibitor and a metal surface, via the high electron density on nitrogen and oxygen atoms, together with the π-electrons of unsaturated bonds and the vacant d-orbital of iron atoms [30]. It is important to highlight that the solubility of the inhibitor in the environments achieves optimum results in the metal surface protection [31]. Coordination compounds containing metal ions with only water as a ligand are called metal aquo-complexes. These complexes are the prevalent chemical structures in aqueous solutions of many metal salts. Metal aquo-complexes have a wide area in the field of environmental, biological, and industrial chemistry [32]. The interaction of water molecules with iron helps us to understand the nature of the subsequent corrosion of iron-based structural materials [33]. Researchers reported that some transition metal ions with organic complexes in an aqueous solution are strong molecular compositions which could be adsorbed on metal surfaces [34, 35]. From what was described earlier, the suggested mechanism route of interaction between inhibitor molecule and metal surface has two steps: first is the approach of two components (L5) to active sites with high electron density N (imine group) for an easy overlap, forming a kind of transition metal complex with Fe^{+2} in a solution; the second step forms a transition metal

complex via high electron density of oxygen atom (C=O group) which can adsorb on the metal surface (see Eq. 8).

$$\begin{aligned} &L5(sol) + [Fe(H_2O)_4]^{+2}(sol) \rightarrow [Fe\,(L5)_2(H_2O)_4]^{+2} \\ &(sol) + Fe(H_2O)_4(ads) \rightarrow [Fe_2(L5)_2(H_2O)_8]^{+2}(ads) \end{aligned} \quad (8)$$

where L5 is the suggested inhibitor (5) in a solution; $[Fe(H_2O)_4]^{+2}$ is the square planar complex in a solution; $[Fe\,(L5)_2(H_2O)_4]^{+2}$ is the octahedral complex in a solution; $Fe(H_2O)_4$ is the square planar complex (H_2O molecules adsorb on metal surface); and $[Fe_2(L5)_2(H_2O)_8]^{+2}$ is the octahedral complex on the metal surface. By using (MM+), and then PM3 semi-empirical calculations, the optimized geometry was determined on L5, $[Fe\,(L5)_2(H_2O)_4]^{+2}$, $[Fe(H_2O)_4]^{+2}$, $Fe(H_2O)_4$ and $[Fe_2(L5)_2(H_2O)_8]^{+2}$ complexes, as shown in Scheme 2.

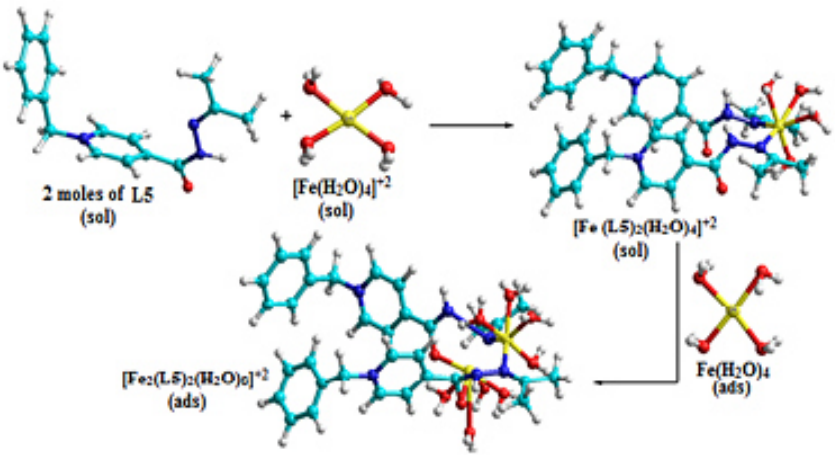

Scheme 2. More energetically stable conformations of the suggested L5, $[Fe\,(L5)_2(H_2O)_4]^{+2}$, $[Fe(H_2O)_4]^{+2}$, $Fe(H_2O)_4$ and $[Fe_2(L5)_2(H_2O)_8]^{+2}$ complexes with PM3 method.

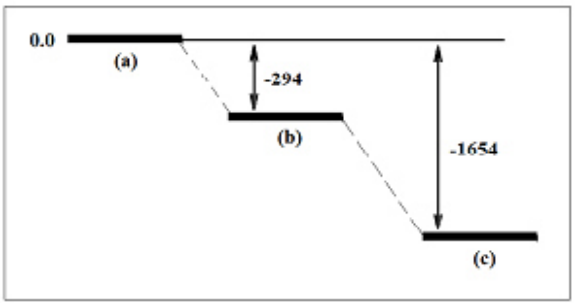

Figure 5. Relative energy diagram for the complexes' formation. (a) (L5 + $[Fe(H_2O)_4]^{+2}$), (b) ($[Fe\,(L5)_2(H_2O)_4]^{+2}$) and (c) ($[Fe_2(L5)_2(H_2O)_8]^{+2}$); energies are in kJ mol^{-1}.

Fig. 5 is the illustrated profile of the relative energy of the complexes' formation by the subtracted part from the sum of the total energy of the isolated components (see Table 3). It's clear from Fig. 4 that the complex's formation proceeds from the soluble $[Fe\,(L5)_2(H_2O)_4]^{+2}$ complex's formation, which is more stable than its components. The complex's formation $[Fe_2(L5)_2(H_2O)_8]^{+2}$

proceeds of the adsorption on the metal surface by shifting the system to the lowest energy.

Table 3. Calculated quantum chemical parameters of the suggested inhibitors, using PM3 method.

Component	E_{total} (kJ/mol)	HOMO (eV)	LUMO (eV)	ΔE^a (eV)	μ(Debye)
L5	-284168.9	-12.2342	-5.7243	6.5100	3.0
$[Fe(H_2O)_4]^{+2}$	-174574.6	-21.9848	-10.3891	11.5957	2.5
$Fe(H_2O)_4$	-176252.6	-6.1094	3.4342	9.5436	0.7
$[Fe\ (L5)_2(H_2O)_4]^{+2}$	-743206.3	-17.7939	-12.0501	5.7438	17.7
$[Fe_2(L5)_2(H_2O)_8]^{+2}$	-921112.7	-17.5200	-11.6145	5.9055	10.4

$^a\Delta E = (E_{LUMO} - E_{HOMO})$

The nature of the complexes' systems is represented by the frontier orbital's energies, as shown in Table 1 and Fig. 6.

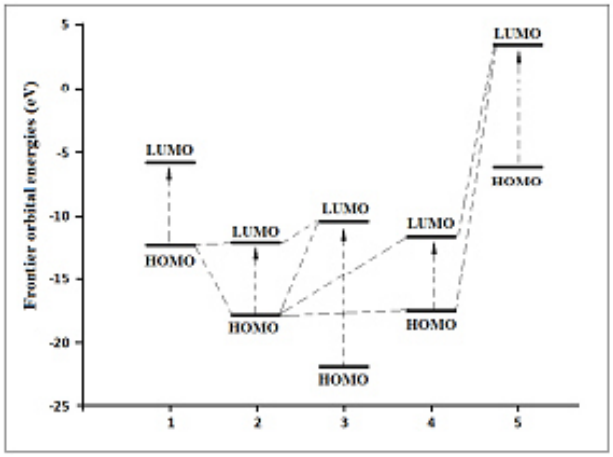

Figure 6. Correlation diagram for the complex's formation 2 ($[Fe\ (L5)_2(H_2O)_4]^{+2}$) from the components 1(L5) and 3($[Fe(H_2O)_4]^{+2}$) and complex's formation 4 ($[Fe_2(L5)_2(H_2O)_8]^{+2}$) from 2 and 5 ($Fe(H_2O)_4$).

Donor-acceptor interactions of these molecular model systems, after investigating the frontier molecular orbitals, show that HOMO, LUMO and ΔE (lower values) energies of L5 and $[Fe\ (L5)_2(H_2O)_4]^{+2}$complex have got donating properties, while $[Fe(H_2O)_4]^{+2}$ and $Fe(H_2O)_4$ complexes have got acceptor properties.

Also, the dipole moment is the ability of the electrons to respond to a changing electric field. Table 3 shows that the dipole moment of molecular complexes $[Fe\ (L5)_2(H_2O)_4]^{+2}$ and $[Fe_2(L5)_2(H_2O)_8]^{+2}$ has different values as compared to their components L5 and, $[Fe(H_2O)_4]^{+2}$and $Fe(H_2O)_4$. This is because of the redistribution of the electron's density occurring in the case of the molecular complex, causing changes in the values of the dipole moment.

It is also possible to add useful information by using the PM3 level of calculations to give a clear picture about the nature of the molecular complexes' systems. Scheme 3 shows the self-organization of $[Fe\ (L5)_2(H_2O)_4]^{+2}$ molecular complex's system, followed by the self-assembly of $[Fe_2(L5)_2(H_2O)_8]^{+2}$ molecular complex's system.

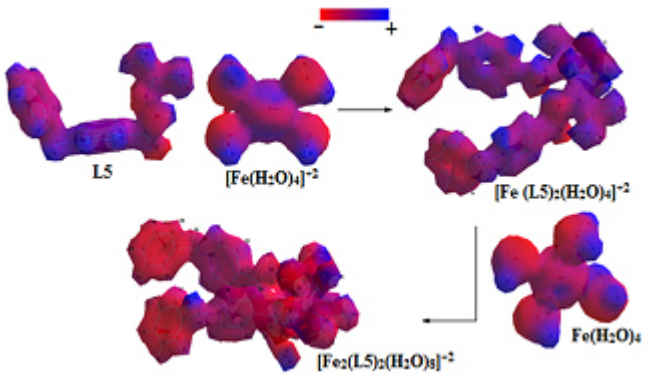

Scheme 3. Electrostatic potential maps for the above suggested components by using PM3 method.

This simple picture explains the nature of the interaction between and among the molecules through the redistribution of the electron's density around $[Fe(L5)_2(H_2O)_4]^{+2}$ and $[Fe_2(L5)_2(H_2O)_8]^{+2}$ molecular complexes' systems and their components. In other words, scheme 3 depicts that non uniform electron's density for all suggested molecular modeling systems is caused by changes in all kinds of energies (see Table 3).

We conclude that theoretical calculations could play an important role in explaining the mechanism route of the organic inhibition protection for the iron metal surface though the suggestion of a simple and proper molecular modeling system, to understand the interaction between the organic molecule and metal surfaces.

Conclusions

The suggested N-pyridinium salt derivatives (1), (2), (3), (4) and (5) were successfully prepared and used as corrosion inhibitors for mild steel in 1 M H_2SO_4 solution at 30 ^oC. The results for the inhibitive efficiency showed excellent inhibiting effects of the suggested inhibitors. The values of the free energy of adsorption revealed a physisorption effect for (1), (2), (3), (4) and (5). Molecular models for prepared compounds (1), (2), (3), (4) and (5) were carried out by using molecular mechanics and semi-empirical molecular orbital calculations. The theoretical calculations gave useful information to explain the mechanism route of interaction between the metal surface and the organic molecules.

Acknowledgments

The authors would like to thank the Department of Chemistry at Al-Nahrain University for its help and cooperation throughout this research.

References

1. Lebrini M, Bentiss F, Vezin H, et al. Corros Sci. 2000;48:1279-1291.
2. Scendo M, Trela J. Int J Electrochem Sci. 2013;8:8329-8347.

3. Silva AB, D'Elica E, Cunha JA, et al. Corros. Sci., 2010;52:788-793.
4. Negm NA, Elkholy YM, Zahran MK, et al. Corros Sci. 2010;52:3523-3536.
5. Jacob KS, Parameswaran G. Corros. Sci. 2010;52:224-228.
6. Heakal FE, Fouda AS, Radwan MS. Mater Chem Phys. 2011;125:26-36.
7. Soror TY, El-Ziady M. Mater Chem Phys.2003;77:697-703.
8. Prathibha BS, Kotteeswaran P, Bheema RV. Res J Recent Sci. 2013;2:1-10.
9. Oguzie EE, Li YS, Wang F. RSC Adv. 2011;1:866-873.
10. Fu JJ, Li SN, Wang Y, et al. J Mater Sci. 2011;45:6255-6265.
11. Issa MR, Khedr MA, Rizk H. J Chinese Chem Soc. 2008;55:875-884.
12. Daeniker HU, Gro CA, Organic Syntheses, Coll. 1973;5:989. 1964;44:86.
13. ASTM G 31- 72. Standard practice for labortary immersion corrosion testing of metals. ASTM: West Conshohocken, PA; 1990.
14. Ajmal M, Mideen AS, Quraishi MA. Corros Sci. 1994;36:79-84.
15. Scendo M, Hepel M. J Electroanalytical Chem. 2008;613:35-50.
16. Elachouri M, Hajji MS, Salem M. Corrosion. 1996;52:103-108.
17. Agrawal R, Namboodhiri TKG. Corros Sci. 1990;30:37-52.
18. Sahin M, Bilgic S, Yilmaz H. Appl Surf Sci. 2009;195:1-9.
19. Chakravarthy MP, Mohana KN. Inter J Corrosion. 2013;1-13.
20. Stewart JPJ. Method J Comput Chem. 1989;10:209-220.
21. HyperChem. Version 7.5. Gainesville, FL: Hypercube Inc; 2002.
22. Khaled KF, Corros Sci. 2010;52:3225-3234.
23. Senhaji O, Taouil R, Skalli MK, et al. Int J Electrochem Sci. 2011;6:6290-6299.
24. Fu JJ, Zang HS, Li SN, et al. Ind Eng Chem Res. 2012;51:6377-6386.
25. Bensajjay E, Alehyen S, El Achouri M, et al. Anti-Corros Meth Mater. 2003;50:402-409.
26. Li X, Deng S, Fu H. Corros Sci. 2009;51:1344-1355.
27. Moretti G, Guidi F, Grion G. Corros Sci. 2004;46:387-403.
28. Saratha R, Meenakshi R. Rasayan J Chem. 2011;4:251-263.
29. Shihab MS, Al-Doori HH. J Mol Struct. 2014;1076:658-663.
30. Feng L, Wang H, Wang F. Electrochim Acta. 2011;58:427-436.
31. Palou RM, Xomelt OO, Likhanova NV. Environmentally Friendly Corrosion Inhibitors. In: Developments in Corrosion Protection. Aliofkhazraei M, editor. Chap. 19. Croatia: In Tech Europe; 2014.
32. Ogden MI, Beer PD. Water & O-Donor Ligands. In: King RB, editor. The Encyclopedia of Inorganic Chemistry. John Wiley & Sons; 2005. p.1-17,
33. Advanced Tribology. Proceedings of CIST2008 & ITS-IFToMM2008. Luo J, Meng Y, Shao T, editors. Springer; 2009. p. 654-657.
34. Fein JB. Environmental Geochemistry, Water-Rock Interactions, Ore Deposits, and Environmental Geochemistry. Hellmann R, Wood SA, editors. The Geochemical Society; 2002. p. 365-378.
35. Jonsson EO, Thygesen KSJ, Ulstrup KW, et al. J Phys Chem B. 2011;115:9410-9416.